A&A 492, 265–275 (2008)
DOI: 10.1051/0004-6361:200810834

Astronomy & Astrophysics

Electron-ion recombination for Fe VIII forming Fe VII and Fe IX forming Fe VIII: measurements and theory

E. W. Schmidt[1], S. Schippers[1], D. Bernhardt[1], A. Müller[1], J. Hoffmann[2], M. Lestinsky[2,3], D. A. Orlov[2], A. Wolf[2], D. V. Lukić[3,⋆], D. W. Savin[3], and N. R. Badnell[4]

[1] Institut für Atom- und Molekülphysik, Justus-Liebig-Universität, Leihgesterner Weg 217, 35392 Giessen, Germany
http://www.uni-giessen.de/cms/iamp e-mail: eike.w.schmidt@iamp.physik.uni-giessen.de
[2] Max-Planck-Institut für Kernphysik, Saupfercheckweg 1, 69117 Heidelberg, Germany
http://www.mpi-hd.mpg.de/ion-storage/
[3] Columbia Astrophysics Laboratory, Columbia University, 550 West 120th, New York, NY 10027, USA
http://www.astro.columbia.edu/~savin/
[4] Department of Physics, University of Strathclyde, Glasgow G4 0NG, UK
http://amdpp.phys.strath.ac.uk/

Received 20 August 2008 / Accepted 9 October 2008

ABSTRACT

The photorecombination rate coefficients of potassium-like Fe VIII ions forming calcium-like Fe VII and of argon-like Fe IX forming potassium-like Fe VIII were measured by employing the merged electron-ion beams method at the Heidelberg heavy-ion storage-ring TSR. New theoretical calculations with the AUTOSTRUCTURE code were carried out for dielectronic recombination (DR) and trielectronic recombination (TR) for both ions. We compare these experimental and theoretical results and also compare with previously recommended rate coefficients. The DR and TR resonances were experimentally investigated in the electron-ion collision energy ranges 0–120 eV and 0–151 eV for Fe VIII and Fe IX. Experimentally derived Fe VIII and Fe IX DR + TR plasma rate coefficients are provided in the temperature range $k_B T$ = 0.2 to 1000 eV. Their uncertainties amount to <±26% and <±35% at a 90% confidence level for Fe VIII and Fe IX, respectively.

Key words. atomic data – atomic processes – plasmas – galaxies: active – galaxies: nuclei – X-rays: galaxies

1. Introduction

Recent spectroscopic observations of active galactic nuclei (AGN) have revealed a broad absorption feature in the X-ray wavelength band 15–17 Å (Sako et al. 2001; Pounds et al. 2001; Kaspi et al. 2002; Behar et al. 2003; Steenbrugge et al. 2003; Kaspi et al. 2004; Gallo et al. 2004; Pounds et al. 2004; Krongold et al. 2005). This absorption feature has been identified as an unresolved transition array (UTA) due mainly to 2p → 3d inner shell absorption in moderately charged iron ions (Fe VII–Fe XVI) with an open M-shell. On the basis of atomic structure calculations and photoabsorption modeling, Behar et al. (2001) point out that the shape of the absorption profile can be used for diagnostics of the AGN absorber. However, Netzer et al. (2003) noted a disagreement between the predicted and observed shape of this feature. As a possible cause for this discrepancy they suggested an underestimation of the low temperature dielectronic recombination (DR) rate coefficients for iron M-shell ions. These rate coefficients together with the radiative recombination (RR) rate coefficients and balanced by photoionization determine the charge level balance of the iron M-shell ions in a photoionized plasma and, consequently, the shape of the UTA (Netzer 2004; Kraemer et al. 2004).

Until recently reliable low temperature DR rate coefficients were not available in the literature for most of the iron M-shell ions. The widely used compilation of Arnaud & Raymond (1992) is largely based on theoretical work by Jacobs et al. (1977) and Hahn (1989). The purpose of this early theoretical work was to produce DR data for modeling collisional ionization equilibrium (CIE). However ions form in CIE (Bryans et al. 2006) at temperatures about an order of magnitude higher than those where they form in photoionized gas (Kallman et al. 2004). Therefore, it is questionable to use these theoretical DR data for modeling photoionized objects.

At the low temperatures where Fe M-shell ions form in photoionized plasmas, theoretical uncertainties in resonance positions of the order of 100 meV can result in order of magnitude uncertainties of the photorecombination rate coefficient (Schippers et al. 2004). As a result modern theory does not always succeed in describing low-energy DR of low to moderately charged ions with sufficient accuracy (Schippers et al. 2002; Badnell 2006b; Lukić et al. 2007; Nikolić et al. 2007). Therefore, benchmarking by experiment is highly desirable. To date, DR measurements of M-shell ions of third- and fourth-row elements have been published for Na-like Fe XVI (Linkemann et al. 1995; Müller 1999), Se XXIV (Pastuszka et al. 1996) and Si IV (Orban et al. 2006; Schmidt et al. 2007), Mg-like Ni XVIII (Fogle et al. 2003) and Fe XV (Lukić et al. 2007), Al-like Fe XIV (Schmidt et al. 2006), and Ar-like Ti V and Sc IV (Schippers et al. 1998, 2002). Schippers (2008) has recently given a bibliographic compilation of storage-ring DR measurements with astrophysically relevant ions. Here and throughout this paper we use the

⋆ *Present address*: Institute of Physics, Pregrevica 118, 11080 Belgrade, Serbia

convention of identifying the recombination process by the initial charge of the ion.

This work presents our experimental photorecombination results using the Heidelberg heavy-ion storage-ring TSR (Müller & Wolf 1997) and our atomic structure calculations using the AUTOSTRUCTURE code (Badnell 1986) for RR + DR + trielectronic recombination (TR Schnell et al. 2003). In particular, we have studied DR and TR of Fe VIII and Fe IX in the electron-ion collision energy ranges 0–120 eV and 0–151 eV, respectively. In these ranges, resonances of the following types are energetically allowed for Fe VIII

$$\mathrm{Fe}^{7+}\left(3s^2\,3p^6\,3d\,\left[^2D_{3/2}\right]\right)+e^-\rightarrow \begin{cases} \mathrm{Fe}^{6+}(3s^2\,3p^6\,3d\,[^2D_{5/2}]\,nl) \\ \mathrm{Fe}^{6+}(3s\;\;3p^6\,3d^2\,nl) \\ \mathrm{Fe}^{6+}(3s^2\,3p^5\,3d^2\,nl) \\ \mathrm{Fe}^{6+}(3s\;\;3p^6\,3d\;\;n^*l^*\,nl) & (n^*\geq 4) \\ \mathrm{Fe}^{6+}(3s^2\,3p^5\,3d\;\;n^*l^*\,nl) & (n^*\geq 4) \\ \mathrm{Fe}^{6+}(3s^2\,3p^6\;\;n^*l^*\,nl) & (n^*\geq 4) \\ \mathrm{Fe}^{6+}(3s\;\;3p^5\,3d^3\,nl) \\ \mathrm{Fe}^{6+}(3s^2\,3p^4\,3d^3\,nl) \end{cases} \quad (1)$$

and for Fe IX

$$\mathrm{Fe}^{8+}\left(3s^2\,3p^6\,[^1S_0]\right)+e^-\rightarrow \begin{cases} \mathrm{Fe}^{7+}(3s\;\;3p^6\,3d\,nl) \\ \mathrm{Fe}^{7+}(3s^2\,3p^5\,3d\,nl) \\ \mathrm{Fe}^{7+}(3s\;\;3p^6\;\;n^*l^*\,nl) & (n^*\geq 4) \\ \mathrm{Fe}^{7+}(3s^2\,3p^5\;\;n^*l^*\,nl) & (n^*\geq 4) \\ \mathrm{Fe}^{7+}(3s\;\;3p^5\,3d^2\,nl) \\ \mathrm{Fe}^{7+}(3s^2\,3p^4\,3d^2\,nl)\,, \end{cases} \quad (2)$$

where n^* and n represent the principal quantum number of the excited core electron and the captured electron, respectively. The published associated excitation energies for the Fe VIII and Fe IX levels, relative to the ground level are listed in Tables 1 and 2, respectively.

The present paper is organized as follows. In Sect. 2 the theory for calculating RR, DR, and TR rate coefficients with AUTOSTRUCTURE is briefly described. In Sect. 3 the experimental procedure is presented. Experimental and theoretical results are given in Sect. 4. The recombination plasma rate coefficients are derived in Sect. 5. A discussion of the data and conclusions of the present work are presented in Sects. 6 and 7, respectively.

Table 1. Available energy levels of Fe VIII relative to the $3p^6\,3d\,(^2D_{3/2})$ ground level.

Level	Energy (eV)
$3p^6\,3d\,(^2D_{5/2})$	0.2276[a]
$3p^5\,(^2P^\circ)\,3d^2\,(^1G)\,^2F^\circ_{5/2}$	53.4682[a]
$3p^5\,(^2P^\circ)\,3d^2\,(^1G)\,^2F^\circ_{7/2}$	53.8779[a]
$3p^5\,(^2P^\circ)\,3d^2\,(^1D)\,^2F^\circ_{7/2}$	55.5025[a]
$3p^5\,(^2P^\circ)\,3d^2\,(^1D)\,^2F^\circ_{5/2}$	56.9542[a]
$3p^5\,(^2P^\circ)\,3d^2\,(^1S)\,^2P^\circ_{3/2}$	63.0482[a]
$3p^5\,(^2P^\circ)\,3d^2\,(^1S)\,^2P^\circ_{1/2}$	64.5737[a]
$3p^6\,4p\,(^2P^\circ_{1/2})$	63.2663
$3p^6\,4p\,(^2P^\circ_{3/2})$	63.9200
$3p^5\,(^2P^\circ)\,3d^2\,(^3F)\,^2F^\circ_{5/2}$	66.4442[a]
$3p^5\,(^2P^\circ)\,3d^2\,(^3F)\,^2F^\circ_{7/2}$	67.1691[a]
$3p^5\,(^2P^\circ)\,3d^2\,(^3P)\,^2P^\circ_{1/2}$	73.3942[a]
$3p^5\,(^2P^\circ)\,3d^2\,(^3P)\,^2P^\circ_{3/2}$	73.7894[a]
$3p^5\,(^2P^\circ)\,3d^2\,(^3F)\,^2D^\circ_{5/2}$	73.9520
$3p^5\,(^2P^\circ)\,3d^2\,(^3F)\,^2D^\circ_{3/2}$	74.0266
$3p^6\,4f\,(^2F^\circ_{5/2})$	94.6871
$3p^6\,4f\,(^2F^\circ_{7/2})$	94.6990
$3p^5\,3d\,(^3P^\circ)\,4s\,(^2P^\circ_{1/2})$	103.857
$3p^5\,3d\,(^3P^\circ)\,4s\,(^2P^\circ_{3/2})$	104.497
$3p^5\,3d\,(^3F^\circ)\,4s\,(^4F^\circ_{7/2})$	105.033
$3p^5\,3d\,(^3F^\circ)\,4s\,(^4F^\circ_{5/2})$	105.374
$3p^5\,3d\,(^3F^\circ)\,4s\,(^4F^\circ_{3/2})$	105.740
$3p^5\,3d\,(^3F^\circ)\,4s\,(^2F^\circ_{7/2})$	106.019
$3p^5\,3d\,(^3F^\circ)\,4s\,(^2F^\circ_{5/2})$	106.703
$3p^5\,3d\,(^3D^\circ)\,4s\,(^4D^\circ_{7/2})$	108.450
$3p^5\,3d\,(^3D^\circ)\,4s\,(^4D^\circ_{5/2})$	108.705
$3p^5\,3d\,(^3D^\circ)\,4s\,(^4D^\circ_{3/2})$	108.793
$3p^5\,3d\,(^3D^\circ)\,4s\,(^4D^\circ_{1/2})$	108.891
$3p^5\,3d\,(^1D^\circ)\,4s\,(^2D^\circ_{5/2})$	108.985
$3p^5\,3d\,(^1D^\circ)\,4s\,(^2D^\circ_{3/2})$	109.273
$3p^5\,3d\,(^1F^\circ)\,4s\,(^2F^\circ_{5/2})$	109.643
$3p^5\,3d\,(^1F^\circ)\,4s\,(^2F^\circ_{7/2})$	110.014
$3p^5\,3d\,(^3D^\circ)\,4s\,(^2D^\circ_{3/2})$	110.236
$3p^5\,3d\,(^3D^\circ)\,4s\,(^2D^\circ_{5/2})$	110.451
$3p^6\,5f\,(^2F^\circ_{5/2})$	114.941
$3p^6\,5f\,(^2F^\circ_{7/2})$	114.946

Levels and energies are taken from the NIST database (Ralchenko et al. 2007). We are unaware of any published data for any of the excited core levels not listed here. [a] These levels were included in the DR calculations.

2. Theory

The first published theoretical DR rate coefficient for Fe VIII that we are aware of is the work of Woods et al. (1981) who used the Burgess formula (Burgess 1965). Arnaud & Raymond (1992) scaled this result to fit the more detailed calculations by Hahn (1989). Theoretical DR rate coefficients for Fe IX have been published by Jacobs et al. (1977) and recently by Badnell (2006a). The Fe IX rate coefficient given by Arnaud & Raymond (1992) was derived by scaling their own rate coefficient calculated with the Burgess formula to the Fe IX result of Hahn (1989).

In our work here, the photorecombination rate coefficient was calculated in the independent processes, isolated resonances approximation (Seaton & Storey 1976), i.e., RR was treated separately from DR + TR. The validity of this approach has been demonstrated by Pindzola et al. (1992). In order to keep the notation simple it should be implicitly understood in the following that DR also comprises TR (and possible higher order resonant processes) wherever these are significant. For example, in recombination of beryllium-like Cl XIV TR has been found to contribute, depending on the plasma temperature, up to 40% to the total photorecombination rate coefficient in a plasma (Schnell et al. 2003).

Total RR rate coefficients for iron M-shell ions Fe IX through Fe XIII were recently given by Badnell (2006a), following Badnell (2006c). Here, the same calculations as in Badnell (2006a) were performed for Fe IX and new calculations for Fe VIII. The present calculations yield Fe VIII and Fe IX RR merged-beams rate coefficients for comparison with the experiment and new Fe VIII RR plasma rate coefficients.

For Fe VIII we have carried out new DR calculations using a state-of-the-art multiconfiguration Breit-Pauli (MCBP) theoretical method as described by Badnell (2006a). For Fe IX we

Table 2. Available energy levels of Fe IX relative to the $3s^2\,3p^6\,(^1S_0)$ ground level.

Level	Energy (eV)
$3s^2\,3p^5\,3d\,(^3P^\circ_0)$	50.3093[a]
$3s^2\,3p^5\,3d\,(^3P^\circ_1)$	50.62462[a]
$3s^2\,3p^5\,3d\,(^3P^\circ_2)$	51.28844[a]
$3s^2\,3p^5\,3d\,(^3F^\circ_4)$	52.79368[a]
$3s^2\,3p^5\,3d\,(^3F^\circ_3)$	53.22776[a]
$3s^2\,3p^5\,3d\,(^3F^\circ_2)$	53.78667[a]
$3s^2\,3p^5\,3d\,(^3D^\circ_3)$	56.48871[a]
$3s^2\,3p^5\,3d\,(^3D^\circ_1)$	57.1091[a]
$3s^2\,3p^5\,3d\,(^3D^\circ_2)$	57.35714[a]
$3s^2\,3p^5\,3d\,(^1D^\circ_2)$	56.63011[a]
$3s^2\,3p^5\,3d\,(^1F^\circ_3)$	57.75536[a]
$3s^2\,3p^5\,3d\,(^1P^\circ_1)$	72.4745[a]
$3s\,3p^6\,3d\,(^3D_1)$	90.1035[a]
$3s\,3p^6\,3d\,(^3D_2)$	90.2059[a]
$3s\,3p^6\,3d\,(^3D_3)$	90.3764[a]
$3s\,3p^6\,3d\,(^1D_2)$	92.9721[a]
$3s^2\,3p^5\,(^2P^\circ_{3/2})\,4s\,(3/2,1/2)^\circ_1$	117.847
$3s^2\,3p^5\,(^2P^\circ_{1/2})\,4s\,(1/2,1/2)^\circ_1$	119.715
$3s^2\,3p^5\,4d\,(^3P^\circ_1)$	148.5603
$3s^2\,3p^5\,4d\,(^1P^\circ_1)$	150.4114

Levels and energies are taken from the NIST database (Ralchenko et al. 2007). We are unaware of any published data for any of the excited core levels not listed here. [a] These levels were included in the DR calculations.

derived a theoretical DR merged-beams rate coefficient by repeating the earlier calculations (Badnell 2006a). In both calculations only the strong $\Delta n^* = 0$ DR + TR channels associated with $3 \rightarrow 3$ core transitions have been considered. The weaker $\Delta n^* \geq 1$ DR channels have been neglected in order to keep the calculation tractable. Δn^* denotes the difference of the principle quantum numbers n^* involved in the core excitation. Details of the MCBP calculations have been reported in Badnell et al. (2003). Briefly, the AUTOSTRUCTURE code was used to calculate energy levels as well as radiative and autoionization rates in the intermediate-coupling approximation. These must be post-processed to obtain the final-state level resolved and total DR data. The ionic thresholds were shifted to known spectroscopic values for the $3 \rightarrow 3$ transitions. Radiative transitions between autoionizing levels were accounted for in the calculation. The DR cross section was approximated by the sum of Lorentzian profiles for all included resonances. The basic configurations which describe the N-electron target for Fe VIII are $3s^2\,3p^6\,3d$, $3s^2\,3p^5\,3d^2$, $3s\,3p^6\,3d^2$, $3s^2\,3p^4\,3d^3$ (and $3s\,3p^5\,3d^3$ for recombination associated with capture into $n = 3$). The Fe IX target configurations are $3s^2\,3p^6$, $3s^2\,3p^5\,3d$, $3s\,3p^6\,3d$, $3s^2\,3p^4\,3d^2$ and $3s\,3p^5\,3d^2$. TR is accounted for via the double core excitations $3s^2\,3p^6\,3d^{(q)} \rightarrow 3s^2\,3p^4\,3d^{(q+2)}$ and $3s^2\,3p^6\,3d^{(q)} \rightarrow 3s\,3p^5\,3d^{(q+2)}$, with $q = 1$ and $q = 0$ for Fe VIII and Fe IX, respectively. Calculations for both ions assume a closed shell Ne-like core.

3. Experimental technique

The experiments were performed utilizing the heavy-ion storage-ring TSR at the Max-Planck-Institut für Kernphysik (MPI-K) in Heidelberg, Germany. The various aspects of the merged-beams technique as used at TSR have been described by Kilgus et al. (1992), Lampert et al. (1996), Pastuszka et al. (1996), Schippers et al. (2001), Wolf et al. (2006), and Lestinsky et al. (2008).

Beams of ^{56}Fe VIII and ^{56}Fe IX were provided by the tandem accelerator of the MPI-K linear accelerator facility at energies of about 1.3 MeV/u and 1.7 MeV/u, respectively. Each charge and mass selected ion beam was injected into the storage-ring and subjected to electron cooling in order to reduce its diameter and initial velocity spread. Ions were accumulated in TSR by multi-turn injection and "ecool stacking" (Grieser et al. 1991). Electrical ion currents of typically 7–12 μA for ^{56}Fe VIII and 2–9 μA for ^{56}Fe IX were achieved. Storing for a few seconds before starting the recombination measurements allowed essentially all metastable Fe VIII and most metastable Fe IX to relax to the ground level.

Argon-like ions with zero nuclear spin such as ^{56}Fe IX have an excited level $3s^2\,3p^5\,3d\,(^3P_0)$ which is forbidden to decay to the ground level $3s^2\,3p^6\,^1S_0$ via a one-photon decay. This means that the lifetime of this level is nearly infinite and there is possibly a fraction of ions in that excited level in the stored ion beam. This leads to an unknown ground level ion current. A similar problem with $^3P_0$ metastable levels was was also seen for DR experiments with beryllium-like ^{56}Fe XXIII (Savin et al. 2006) and magnesium-like ^{56}Fe XV (Lukić et al. 2007). Due to the rich and complex DR-spectrum of Fe IX an estimation of the metastable fraction in the DR spectrum by comparing experiment and theory was not successful. Therefore we follow the approach of Lukić et al. (2007) to estimate of the metastable fraction in the ion beam to be 6% ± 6%. Correspondingly, the measured Fe IX ion current was multiplied by a factor of 0.94 in order to represent the ground-state fraction. DR resonances from the metastable ions could not be identified and their influence is treated only as an uncertainty of the determined plasma rate coefficient for ground-state ions (see Sect. 5.1).

In the present experiment a newly installed separate merged electron beam device (Sprenger et al. 2004) was used in addition to the previously used electron cooler. This additional electron beam is hereafter denoted as the electron target. As in the electron cooler, the electron beam of the electron target is also guided by a magnetic field and overlaps the ion beam over a straight section of ≈1.5 m length. Conceptually the experimental procedures for measuring recombination rate coefficients with the electron target are the same as those that were applied previously with the electron cooler. However, there are advantages when both an electron cooler and a separate electron target are used for recombination measurements. First, the electron cooler can be used to continuously cool the ion beam. Thus, the low velocity and spatial spread of the ion beam is maintained at all times. Second, the electron target was specifically designed for providing an electron beam with a very low initial energy spread (Sprenger et al. 2004). Both measures yield a higher experimental resolution in the present measurement as compared to previous measurements with the electron cooler (Wolf et al. 2006; Schmidt et al. 2007).

Recombined ions in the electron target were separated from the parent beam in the first dipole magnet behind the electron target and counted using a single particle scintillation counter with a nearly 100% detection efficiency. During the recombination measurement, the laboratory energy of the electron target beam was chopped between the energies for measurement (E_m) and reference ($E_r^{(m)}$), both with a 10 ms duration of data collection. Between the voltage jump and the data collection there was a settling time of 10 or 12.5 ms to allow the power supplies to reach the preset values. The superscript (m) in $E_r^{(m)}$ indicates

that the background is recorded in every energy scan separately for each measurement energy E_m. The data for Fe VIII and Fe IX were collected in 38 and 23 overlapping data sets from E_m = 699 to 1 470 eV and from E_m = 910 to 1 560 eV, respectively. For each data set E_m was changed in the laboratory frame by 0.12 eV with each step in the chopping pattern whereas $E_r^{(m)}$ was kept fixed at an energy usually where no significant contribution by DR to the recombination signal was expected. Under this condition the recombination rate measured at $E_r^{(m)}$ allows us to determine the background recombination signal due primarily to electron capture off the residual gas in TSR. The merged-beams rate coefficient is derived from the background subtracted recombination count rate as follows (Poth et al. 1988; Kilgus et al. 1992; Schippers et al. 2001)

$$\alpha(E_m) = \frac{\left[R(E_m) - R\left(E_r^{(m)}\right)\right]}{(1-\beta_i\beta_e)\eta n_e(E_m) N_i L/C} + \alpha\left(E_r^{(m)}\right)\frac{n_e\left(E_r^{(m)}\right)}{n_e(E_m)}, \qquad (3)$$

where R is the recombination count rate, η the detection efficiency, n_e the electron density in the interaction region, N_i the number of ions in the ring, and C = 55.4 m the circumference of the TSR. The nominal length L of the electron-ion overlap region in the electron target section is L = 1.476 m. The ion velocity and the electron velocity are $v_i = \beta_i c$ and $v_e = \beta_e c$, respectively, where c is the speed of light. The second term in Eq. (3) is a small correction that re-adds the recombination rate coefficient at the reference point $\alpha(E_r^{(m)})$. Typically it was taken to be the theoretical rate coefficient for RR calculated by using the AUTOSTRUCTURE code and applying a field ionization model (cf. Sect. 4). In some cases it had to be derived from the total measured recombination rate coefficient of a data set with a different reference energy. As the final step of the data analysis a deconvolution procedure was applied that accounts for the contributions to the measured rate coefficient by the merging and de-merging sections in the toroidal magnetic fields of the electron target (Lampert et al. 1996). The systematic experimental uncertainty of the merged-beams rate coefficient is estimated to be ±25% at a 90% confidence level (Lampert et al. 1996). This uncertainty stems mostly from the ion current measurement. Additional uncertainties discussed below result in a higher total experimental uncertainty, as is explained in Sect. 5. Unless stated otherwise all uncertainties in this paper are cited at a 90% confidence level.

The relative electron-ion collision energy $\hat{E}$ was derived from the laboratory energies E_m and the target energy E_c for fulfilling the electron-ion velocity-matching condition (Kilgus et al. 1992), which was $E_c \approx 716$ eV and $E_c \approx 933.6$ eV for Fe VIII and Fe IX, respectively. The experimental electron energy distribution is best described as a flattened Maxwellian distribution which is characterized by the longitudinal and transverse temperatures $T_\parallel$ and $T_\perp$ (Kilgus et al. 1992). The experimental energy resolution is approximately given by $\Delta\hat{E} = [(\ln(2)\, k_B T_\perp)^2 + 16\ln(2)\,\hat{E} k_B T_\parallel]^{1/2}$. To reduce $T_\perp$ the target electron beam was adiabatically expanded (Pastuszka et al. 1996) by a factor of 30. Starting from a cathode temperature of about 1300 K the transversal temperature after expansion is expected to be $k_B T_\perp \approx 3.7$ meV which is in agreement with the low energy fits discussed later in Sect. 5. Typically, the longitudinal temperature can be deduced from the width of a gaussian line shape fitted to a single narrow resonance at an energy where the experimental peak width is dominated by $k_B T_\parallel$. For the present cases of Fe VIII and Fe IX all resonance shapes are unresolved blends of several DR resonances. Therefore, the longitudinal temperatures were estimated by fitting the convoluted theoretical DR line profiles from the AUTOSTRUCTURE calculation to the measured spectrum in the electron ion collision energy ranges 67.7–72.1 eV for Fe VIII and 65.3–70.3 eV for Fe IX. This yields $k_B T_\parallel$ = 33.4(3) μeV and 34.9(3) μeV, respectively. With the above given temperature values, the experimental energy spread for both ions thus amounts to $\Delta\hat{E} \approx 0.007$ eV at $\hat{E}$ = 0.1 eV, $\Delta\hat{E} \approx 0.02$ eV at 1 eV, $\Delta\hat{E} \approx 0.06$ eV at 10 eV, and $\Delta\hat{E} \approx 0.2$ eV at 100 eV.

4. Experimental and theoretical results

The experimentally derived and theoretically calculated recombination merged-beams rate coefficients are presented separately for Fe VIII and Fe IX in the following sections. To compare experimental and theoretical results, one has to take into account the field ionization of high Rydberg levels in the storage-ring bending magnets and the experimental energy spread. Field ionization of the loosely bound high Rydberg electron in the recombined ions can result from the motional electric fields that the moving ions experience inside the storage-ring magnets (Schippers et al. 2001). The strongest magnetic field is that of the bending dipole magnets. In the present experiments, only Rydberg levels with quantum numbers less than $n_{cut} \approx 32$ (34) for Fe VIII (Fe IX) were not ionized in the dipole magnet. The field ionization of ions in Rydberg levels with $n \geq n_{cut}$ is sufficiently well understood and can be accounted for by a model calculation which also includes the radiative decay of excited ions on their way from the target to the dipole magnet (Schippers et al. 2001). For a meaningful comparison with the experimental results, the theoretical AUTOSTRUCTURE calculations have been combined with the result of the field ionization model.

The theoretical DR and RR rate coefficients were derived by convolving the theoretical cross sections with the experimental electron energy distribution (Kilgus et al. 1992). For the comparison of the AUTOSTRUCTURE DR merged-beams rate coefficients with the experiment we derived a measured DR merged-beams rate coefficient by subtracting the field ionized AUTOSTRUCTURE RR merged-beams rate coefficient from the measured photorecombination merged-beams rate coefficient. Note that unlike for iron L-shell ions where theory and experiment seem to converge in resonance position and relative strength above a few eV, for Fe VIII and Fe IX theory and experiment do not agree in resonance structure until about 55 eV. Similar behavior was seen for the M-shell ions Fe XIV (Schmidt et al. 2006) and Fe XV (Lukić et al. 2007).

4.1. Fe VIII *recombination merged-beams rate coefficients*

Figures 1 and 2 show the measured Fe VIII photorecombination merged-beams rate coefficient in the energy ranges 0–77 eV and 74–120 eV, respectively. In the 0–77 eV range the spectrum is mainly dominated by resonances associated with $3p^6\,3d \rightarrow 3p^5\,3d^2$ one-electron core excitations. Series limits associated with Rydberg series are discernible at $\hat{E}$ = 66.4, 73.4, and 74.0 eV and are mainly associated with 3p excitations from the $3p^6 3d\,(^2D_{3/2})$ level to the $3p^5(^2P^\circ)3d^2(^3F)\,^2F^\circ_{5/2}$, $3p^5(^2P^\circ)3d^2(^3P)\,^2P^\circ_{1/2}$, and $3p^5(^2P^\circ)3d^2(^3F)\,^2D^\circ$ levels, respectively. In the measured spectrum there is no $3p^5(^2P^\circ)3d^2(^3F)\,^2F^\circ_{7/2}$ series limit discernible at $\hat{E}$ = 67.2 eV. There is only weak evidence of resonances belonging to the $3p^5(^2P^\circ)3d^2(^3P)\,^2P^\circ_{3/2}$ Rydberg series. The fine-structure splitting of the ^2D term is not resolved.

In the 74–120 eV range the spectrum is mainly due to resonances connected to $3p^6\,3d \rightarrow 3p^6\,4f$ and $3p^6\,3d \rightarrow 3p^6\,5f$ core excitations. The Rydberg series limits discernable at $\hat{E}$ = 94.7

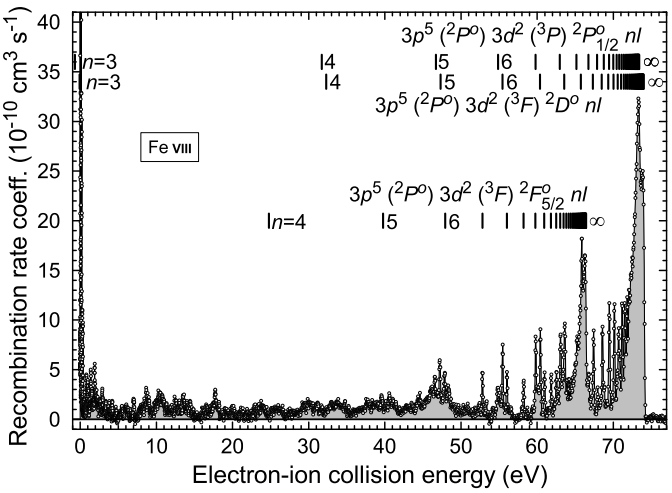

Fig. 1. Measured Fe VIII electron-ion photorecombination merged-beams rate coefficient in the energy range of DR resonances mainly associated with 3p → 3d core excitations. The vertical bars denote DR resonance positions associated with the dominant excitations as expected on the basis of the hydrogenic Rydberg formula.

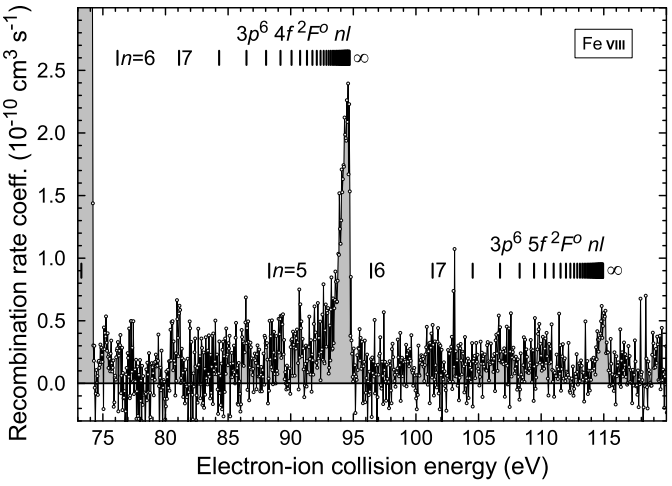

Fig. 2. Measured Fe VIII electron-ion photorecombination merged-beams rate coefficient in the energy range of DR resonances associated with 3d → 4f and 3d → 5f core excitations. The vertical bars denote DR resonance positions as expected on the basis of the hydrogenic Rydberg formula.

and 114.9 eV (Fig. 2) are associated with 3d → 4f and 3d → 5f core excitation, respectively. Resonances and series limits associated with 3p → 4s core excitations are not visible.

The experimental electron-ion collision energy scale was fine tuned by comparing the measured spectrum in the energy range 65–75 eV with the AUTOSTRUCTURE calculation which in turn was energy calibrated to the $3p^6\,3d \rightarrow 3p^5\,3d^2$ transition energies given in the NIST database (Ralchenko et al. 2007). The calibration factor for the experimental electron-ion collision energy deviated by less than 1% from unity.

A detailed comparison between experiment and theory for Fe VIII is shown in Fig. 3, where the theoretical DR rate coefficient was multiplied by a factor of 0.73 over the entire energy range, leading to a scaled theoretical DR merged-beams rate coefficient $\alpha^{\rm DR}_{\rm theo,scaled}$, in order to bring theory into quantitative agreement with the measured DR rate coefficient approaching the strong build up of resonance strength towards the $3p^5(^2P^\circ)3d^2(^3P)\,^2P^\circ$ and $3p^5(^2P^\circ)3d^2(^3F)\,^2D^\circ$ series limits. This scaling factor was derived by fitting the theoretical rate

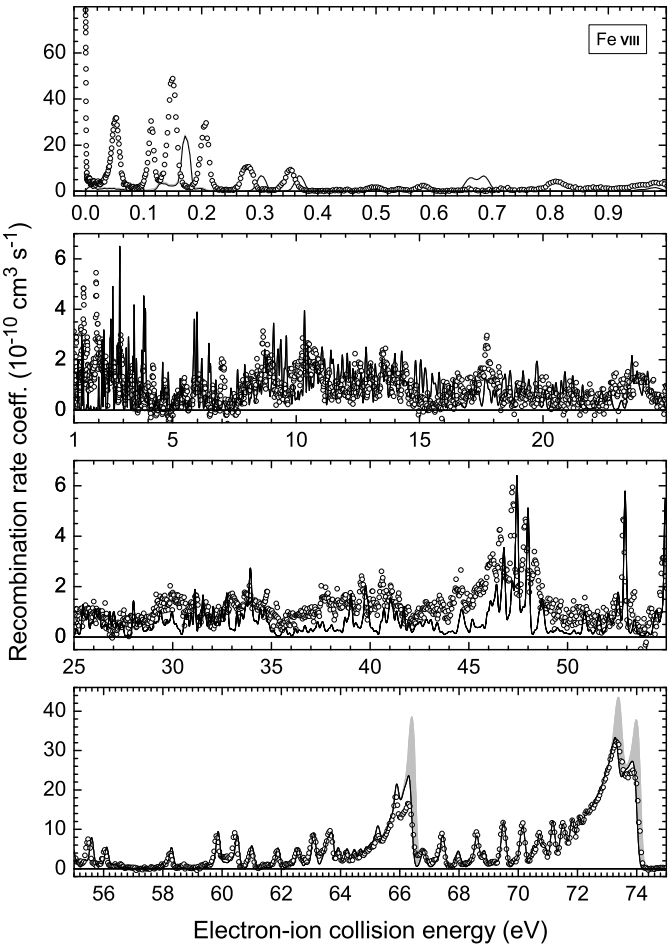

Fig. 3. Comparison between the measured (open circles) and the theoretical Fe VIII DR merged-beams rate coefficient. The calculated rate coefficients were multiplied by a factor of 0.73 (see text). The solid line shows the scaled AUTOSTRUCTURE calculation including the field ionization model of Schippers et al. (2001). The gray shaded area show the additional contribution to the (also scaled) AUTOSTRUCTURE calculation when field ionization is not taken into account. The gray shaded area due to $3p^6\,3d\,(^2D_{3/2}) \rightarrow 3p^6\,3d\,(^2D_{5/2})$ fine structure excitation below 0.3 eV is so small, that it is hardly visible at the given scale.

coefficient to the experimental one in the energy range 67.7–72.2 eV. The factor is not within the total experimental uncertainty of 25%. A similar discrepancy between experiment and theory was found earlier for Fe XIV (Badnell 2006b) and Fe XV (Lukić et al. 2007).

For DR associated with the $3p^6\,3d\,(^2D_{3/2}) \rightarrow 3p^6\,3d\,(^2D_{5/2})$ fine structure excitation the smallest energetically possible Rydberg level which can be populated is $n = 56$, according to the Rydberg formula. The $3p^6\,3d\,(^2D_{5/2})\,56l$ DR resonance would appear at about 0.015 eV in the DR spectrum. However, this Rydberg quantum number is far above the critical field ionization quantum number $n_{\rm cut} \approx 32$ for Fe VIII. Therefore, recombination due to $3p^6\,3d\,(^2D_{3/2}) \rightarrow 3p^6\,3d\,(^2D_{5/2})$ fine structure excitation is not visible in the experiment and the AUTOSTRUCTURE calculation with field ionization model. Anyhow, the calculation without field ionization suggests a negligible fraction of fine structure DR.

In Fig. 3, strong low-energy resonances appear in the measured spectrum at $\hat{E} < 0.5$ eV. The measurements also suggest the existence of at least one resonance below $\hat{E} = 0.001$ eV which will be discussed in Sect. 5.1. Between 0.001–0.5 eV we find resonances in the measured spectrum specifically at

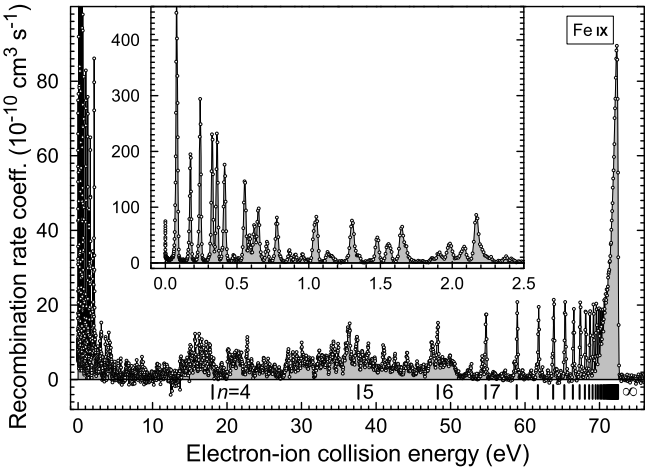

Fig. 4. Measured Fe IX electron-ion photorecombination merged-beams rate coefficient in the energy range of DR resonances mainly associated with $3p^6 \rightarrow 3p^5\,3d$ core excitations. The vertical bars denote DR resonance positions associated with $3s^2\,3p^5\,3d\,(^1P^\circ_1)$ excitation as expected on the basis of the hydrogenic Rydberg formula. The inset shows the low energy region of the measured spectrum in more detail.

$\hat{E}$ = 0.05, 0.11, 0.15, 0.20, 0.28, and 0.35 eV. Their resonance strengths are about an order of magnitude larger than the strengths of any other resonance in the remaining spectrum. Although the AUTOSTRUCTURE calculation includes DR and TR, it does not reproduce the experimentally observed low-energy resonance structure in every detail (upper panel of Fig. 3). But it suggests that the resonances are mainly due to two-electron promotions with capture into $n = 3$ leading to autoionizing $3s^2\,3p^4\,3d^4$ and $3s\,3p^5\,3d^4$ configurations. One electron promotions with capture into $n = 3$ are not possible as all $3s^2\,3p^5\,3d^3$ doubly excited levels are bound and hence are not accessible by pure DR. This means that the strong Fe VIII resonances below 0.4 eV are most probably due to TR. Integrating both DR rate coefficients over the interval 0.001–0.5 eV yields $\int \alpha^{\rm DR}_{\rm theo,scaled} / \int \alpha^{\rm DR}_{\rm exp} = 0.28$.

At energies $\hat{E} \geq 0.5$ eV the agreement between experiment and calculation is mixed. In the range 0.5–5 eV there is resonance strength missing in the calculated rate coefficient. Integrating both DR merged-beams rate coefficients over the interval 0.5–5 eV yields $\int \alpha^{\rm DR}_{\rm theo,scaled} / \int \alpha^{\rm DR}_{\rm exp} = 0.75$. Better agreement is found between 5 and 25 eV. Integrating over this range yields $\int \alpha^{\rm DR}_{\rm theo,scaled} / \int \alpha^{\rm DR}_{\rm exp} = 1.04$. In the range 25–55 eV the agreement is less good again. A significant quantity of resonance strength is missing in the calculation, leading to $\int \alpha^{\rm DR}_{\rm theo,scaled} / \int \alpha^{\rm DR}_{\rm exp} = 0.55$. Beyond 55 eV, not surprisingly the scaled calculation with the field ionization model applied agrees very well with the measurement ($\int \alpha^{\rm DR}_{\rm theo,scaled} / \int \alpha^{\rm DR}_{\rm exp} = 1.02$ in the interval 55–75 eV).

4.2. Fe IX *recombination merged-beams rate coefficients*

Figure 4 shows the measured Fe IX photorecombination merged-beams rate coefficient in the energy range 0–76 eV. This range exhibits resonances associated with $3p^6 \rightarrow 3p^5\,3d$ core excitations. The Rydberg series associated with core excitation into the $3p^5\,3d\,^1P^\circ_1$ level converges to its series limit at $\hat{E}$ = 72.5 eV. In principle, series limits of the $3s\,3p^6\,3d\,(^3D)\,nl$ and $3s\,3p^6\,3d\,(^1D_2)\,nl$ Rydberg series can be expected to occur at $\hat{E}$ = 90.27 eV and $\hat{E}$ = 92.97 eV, respectively (total angular momentum weighted averages; Ralchenko et al. 2007). However, these are not seen in the experimental spectrum. Note that for Fe IX all $3s^2\,3p^5\,3d^2$ doubly excited levels are bound and hence are not accessible by DR. This is in contrast with DR of the isoelectric Sc IV (Schippers et al. 2002) and Ti V (Schippers et al. 1998) where these levels are autoionizing and, thus, contribute to the DR process.

The experimental electron-ion collision energy scale was fine tuned by comparing the measured spectrum in the energy range 66.0–70.3 eV with the AUTOSTRUCTURE calculation which in turn was energy calibrated to the $3p^6 \rightarrow 3p^5\,3d$ transition energies from the NIST database (Ralchenko et al. 2007). The calibration factor for the experimental electron-ion collision energy scale deviated by less than 0.2% from unity.

A detailed comparison between experiment and theory is shown in Fig. 5, where the theoretical DR rate coefficient had to be multiplied with a factor of 0.93 over the entire energy range, in order to bring theory into quantitative agreement with the measured DR rate coefficient in the energy range 63–71 eV just below the $3p^5\,3d\,^1P^\circ_1$ series limit. This factor is within the total experimental uncertainty of 25%.

Strong low-energy resonances appear below $\hat{E}$ = 2.5 eV (Fig. 5). Their resonance strengths are several times larger than the strength of any other resonance in the remaining spectrum. Although the AUTOSTRUCTURE calculation does not reproduce the experimentally observed low-energy resonance structure (upper two panels of Fig. 5) it suggests that it is due to DR associated with $3p^6 \rightarrow 3p^5\,3d$ core excitation and simultaneous capture into $n = 4$.

The agreement between experiment and calculation is mixed. In the range 0.001–2.5 eV there is resonance strength missing in the calculated rate coefficient. Integrating both DR rate coefficients over the interval 0.001–2.5 eV yields $\int \alpha^{\rm DR}_{\rm theo,scaled} / \int \alpha^{\rm DR}_{\rm exp} = 0.49$. This is possibly partly caused by a fraction of DR rate coefficient associated with excitations from the metastable $^3P_0$ ion fraction of the ion beam. Note, though, that the strength of the DR contribution onto the $^3P_0$ metastable will diminish above ~0.32 eV where the autoionization channel to the $^3P_1$ level opens up and further decrease above ~0.98 eV when the $^3P_2$ autoionization channel opens up (for a more detailed explanation of this see Lukić et al. 2007). In contrast to that, there is too much resonance strength in the calculation in the range 2.5–6 eV, where the ratio between experiment and scaled calculation is $\int \alpha^{\rm DR}_{\rm theo,scaled} / \int \alpha^{\rm DR}_{\rm exp} = 1.43$. Integration over the ranges 6–20 eV and 20–58 eV yields $\int \alpha^{\rm DR}_{\rm theo,scaled} / \int \alpha^{\rm DR}_{\rm exp} =$ 0.44 and 0.48, respectively. Beyond 58 eV, not surprisingly the scaled calculation with the field ionization model applied, agrees very well with the measurement ($\int \alpha^{\rm DR}_{\rm theo,scaled} / \int \alpha^{\rm DR}_{\rm exp} = 1.01$ in the interval 58–73 eV).

In addition to the data presented in Figs. 4 and 5, the energy ranges 85–94, 113–122, and 141–151 eV were also experimentally investigated, to search for Rydberg series limits of DR associated with $3s \rightarrow 3d$ and $3p \rightarrow 4l$ excitations. No evidence for these series limits was found within an upper limit for the rate coefficient of 1.5×10^{-10} cm^{3}s^{-1}.

5. Plasma recombination rate coefficients

DR rate coefficients for a Maxwellian plasma can be derived from both the experimental photorecombination merged-beams rate coefficient and the theoretical cross section. This is done in

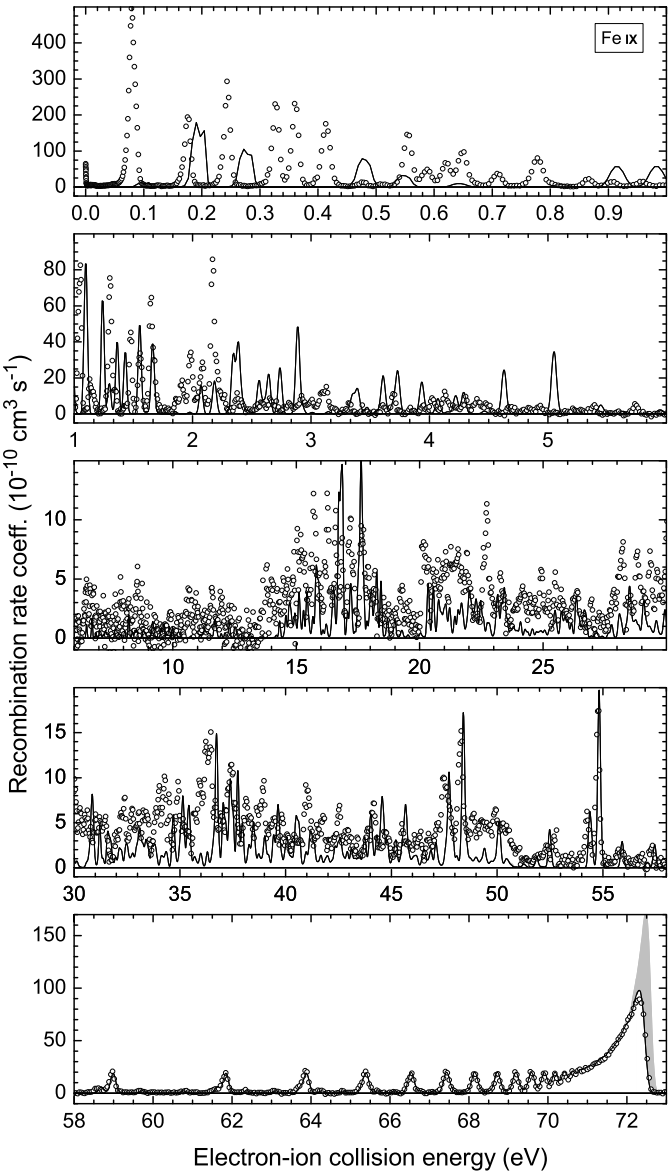

Fig. 5. Comparison between the measured (open circles) and the theoretical Fe IX DR merged-beams rate coefficient. The calculated rate coefficients were multiplied by a factor of 0.93 (see text). The solid line shows the scaled AUTOSTRUCTURE calculation including the field ionization model of Schippers et al. (2001). The gray shaded area shows the additional contribution to the (also scaled) calculation when field ionization is not taken into account.

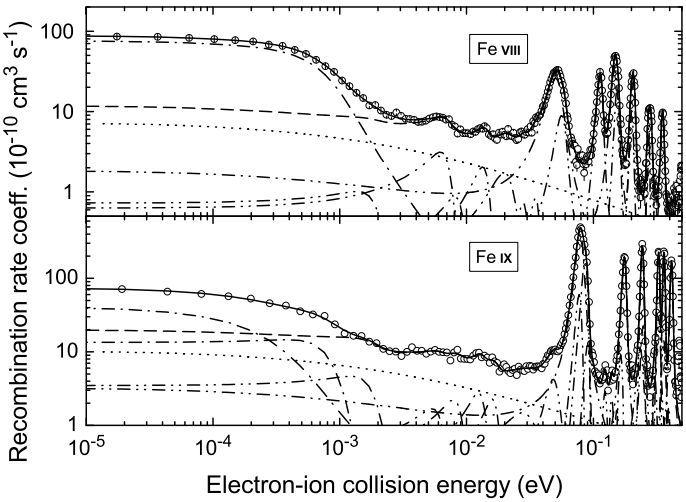

Fig. 6. Measured Fe VIII (*upper panel*) and Fe IX (*lower panel*) photorecombination merged-beams rate coefficient at energies below 0.5 eV (open circles). The solid line is the sum of the Fe VIII (Fe IX) AUTOSTRUCTURE RR calculation (dotted curve, field ionization included) and a fit comprising 18 (28) DR resonances. The dash-dotted curve is the lowest-energy resonance (are the two lowest-energy resonances) of the Fe VIII (Fe IX) resonance fit. The dashed curve is the sum of the remaining 17 (26) fitted resonances (dash-dot-dotted curves) and the Fe VIII (Fe IX) AUTOSTRUCTURE RR calculation.

the following sections. Of particular interest for modeling astrophysical environments are the DR plasma rate coefficients in the electron temperature ranges where Fe VIII and Fe IX form in astrophysical plasmas. The approximate temperature ranges where they form in photoionized and collisionally ionized plasmas can be obtained from the works of Kallman et al. (2004) and Bryans et al. (2006), respectively. For photoionized plasmas, Kallman et al. (2004) find that the fractional Fe VIII (Fe IX) abundance peaks at a temperature of 1.7 eV (1.8 eV). The "photoionized zone" may be defined as the temperature range where the fractional abundance of a given ion exceeds 10% of its peak value. For Fe VIII (Fe IX) this corresponds to a temperature range of 1.1–2.1 eV (1.3–2.3 eV). Using the same criterion and the fractional abundances of Bryans et al. (2006), for coronal equilibrium the Fe VIII (Fe IX) "collisionally ionized zone" is estimated to extend over a temperature range of 17–80 eV (25–107 eV). It should be kept in mind that these temperature ranges are only indicative. They depend, in part, on the accuracy of the underlying atomic data base.

5.1. Derivation of the DR plasma rate coefficients

A DR plasma rate coefficient is derived by convolving the measured DR merged-beams rate coefficient with a Maxwell-Boltzmann electron energy distribution. As detailed by Schippers et al. (2001, 2004), there are three issues that require special consideration: the experimental energy spread, the recombination rate enhancement at low energies, and field ionization of high Rydberg levels in the storage-ring bending magnets. The measured DR merged-beams rate coefficient was derived by subtracting the field ionized AUTOSTRUCTURE RR merged-beams rate coefficient from the measured photorecombination merged-beams rate coefficient.

The experimental energy spread $\Delta\hat{E}$ influences the outcome of the convolution for resonances with resonance energies $\hat{E} \lesssim \Delta\hat{E}$. This can be circumvented by extracting the DR cross section from the measured photorecombination merged-beams rate coefficient at low energies. This was achieved by fitting DR resonance line-shapes plus the calculated field ionized RR merged-beams rate coefficient to the measured spectrum for the energy range 0.01 meV–0.4 eV and 0.01 meV–0.45 eV for Fe VIII and Fe IX, respectively, and is shown in Fig. 6. It should be noted that all of the fitted DR line-shapes are expected to comprise a blend of resonances.

Below 1 meV one typically finds an enhanced recombination rate coefficient in merged electron-ion beam experiments. This is caused by additional recombination in time dependent external fields during the merging of the electron and the ion beams and depends on the electron beam temperatures, ion species, and the electron target's geometry and magnetic field

(Gwinner et al. 2000; Hörndl et al. 2006). It does not contribute to the plasma rate coefficient and therefore has to be removed before further derivation of the recombination plasma rate coefficient. For measurements using the TSR cooler as the electron target, enhancement factors are typically in the range of $(\Delta\alpha/\alpha_0) + 1 = 1.5$–$3$ (Wolf & Gwinner 2003), where α_0 is the theoretically expected value (in most investigated cases only a RR contribution) and $\Delta\alpha$ is the contribution by enhancement (for details see Gwinner et al. 2000). For the TSR target there are no systematic investigations of the rate enhancement yet available. As shown recently (Schmidt et al. 2006) the derivation of an absolute value for the rate enhancement can become rather troublesome when there are DR resonances below 1 meV. With the given experimental resolution, it is impossible to obtain the absolute contribution of resonances below 1 meV and the rate enhancement to the rate coefficient at the same time. Hence, we consider the results for two cases to derive an upper limit for the rate enhancement, either keeping all 18 or 28 fitted resonances (Fig. 6) for Fe VIII and Fe IX, respectively, or removing the resonances below 1 meV, corresponding to including the remaining 17 (26) resonances for Fe VIII (Fe IX). Comparing the resonance fit without resonances below 1 meV (dashed lines in Fig. 6) and the measured rate coefficient at 0.01 meV we find $\alpha_{\rm exp}/\alpha_{\rm fit}^{\rm wo} \approx 7.5$ for Fe VIII and ≈3.7 for Fe IX as an upper limit for the rate enhancement. Total DR plasma rate coefficients $\alpha_{\rm P}^{\rm wi}$ and $\alpha_{\rm P}^{\rm wo}$ were derived from the fits with and without resonances below 1 meV, respectively, for both ions. Their mean values give the resulting experimentally derived plasma rate coefficients and their relative difference is taken as an experimental uncertainty associated with the rate enhancement and is large only at low plasma temperatures. For Fe VIII this uncertainty is ≈47% at $k_{\rm B}T = 0.01$ eV, ≈1.5% at 0.1 eV, and less than 1% above 0.15 eV. For Fe IX it is ≈25% at $k_{\rm B}T = 0.01$ eV, and less than 1% above 0.04 eV. It should be noted that the uncertainty associated with the rate enhancement is negligible in the temperature ranges where Fe VIII and Fe IX exist in either a photoionized or a collisionally ionized plasma (Figs. 7 and 8).

Similar to the approach of Schippers et al. (2001, 2004) the missing DR resonance strength due to field ionization was estimated from the scaled AUTOSTRUCTURE results for n up to $n_{\rm max} = 1000$. Although the AUTOSTRUCTURE code fails to reproduce the resonance structure at low energies it reproduces the more regular resonance structures of Rydberg resonances near the series limits when scaled to the experiment. The unmeasured contributions due to field ionization were derived from the differences between the scaled calculations with $n_{\rm max} = 1000$ and the scaled calculations including the field ionization model. These differences are represented as the gray shaded areas in Figs. 3 and 5. The statistical uncertainty in the scaling of the calculation is below 1%. The unmeasured contributions due to field ionization to the Fe VIII and Fe IX plasma rate coefficients are shown as dotted lines in Figs. 7 and 8, respectively. The missing DR resonance strength due to field ionization contributes less than 12% to the total DR plasma rate coefficient in the temperature range 1 meV–100 keV for both ions. Multiplying these 12% with the 1% scaling uncertainty mentioned above, this leads to an additional uncertainty for the DR plasma rate coefficient of far less than 1% and which is negligible compared to other uncertainties. Due to the small contribution of DR associated with $3{\rm d} \rightarrow n^*l^*$ ($n^* \geq 4$) in the DR rate coefficient of Fe VIII and the missing evidence of DR associated with $3{\rm s} \rightarrow 3{\rm d}$ and $3{\rm p} \rightarrow 4l$ excitation for Fe IX, no correction for field ionization of DR associated with $3{\rm s} \rightarrow 3{\rm d}$, $3{\rm p} \rightarrow 4l$ and $3{\rm d} \rightarrow n^*l^*$ ($n^* \geq 4$) excitations was applied.

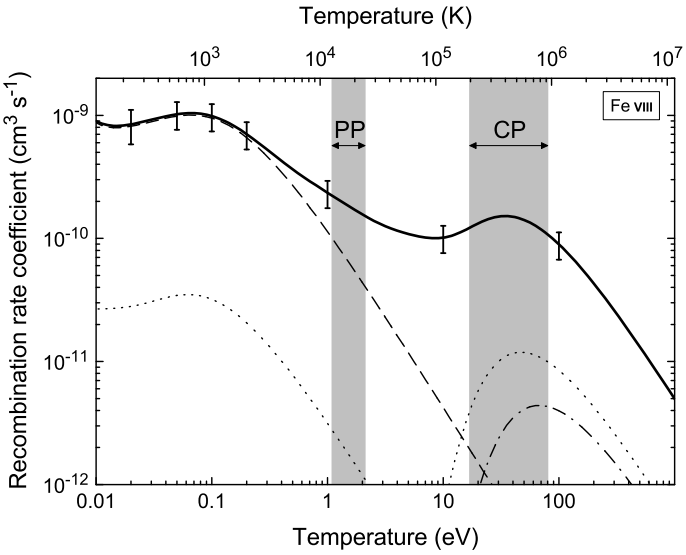

Fig. 7. Experimentally-derived Fe VIII DR rate coefficient in a plasma (full curve) comprising DR associated with $3{\rm p} \rightarrow 3{\rm d}$ ($\Delta n^* = 0$) core excitations (Fig. 1) and DR associated with $3{\rm d} \rightarrow 4{\rm f}$ and $3{\rm d} \rightarrow 5{\rm f}$ ($\Delta n^* = 1$ and $\Delta n^* = 2$) core excitations (Fig. 2). The error bars denote the uncertainty of the absolute rate coefficient at a 90% confidence level. Temperature ranges are highlighted where Fe VIII is expected to peak in abundance in photoionized plasma (PP) and collisionally ionized plasmas (CP). The estimated (unmeasured) DR contribution of levels with $n \geq 32$ (gray shaded area in Fig. 3) is shown by the dotted curves, where the left curve is due to $3{\rm p}^6\,3{\rm d}\,(^2{\rm D}_{3/2}) \rightarrow 3{\rm p}^6\,3{\rm d}\,(^2{\rm D}_{5/2})$ fine structure excitation and the right curve is due to $3{\rm p}^6\,3{\rm d} \rightarrow 3{\rm p}^5\,3{\rm d}^2$ excitation. The dashed curve shows the contribution of the 18 fitted low-energy resonances (upper panel of Fig. 6). The dash-dotted curve shows the contribution by the $\Delta n^* = 1$ and $\Delta n^* = 2$ DR above $\hat{E} = 74.5$ eV.

For Fe IX there are two kinds of uncertainty in the total DR plasma rate coefficient due to the metastable fraction in the ion beam. The first one is the additional ±6% uncertainty in the ground level ion current due to metastable ions in the ion beam. The second one stems from the fraction of DR resonances in the measured spectrum due to DR from the excited $3{\rm s}^2\,3{\rm p}^5\,3{\rm d}\,(^3{\rm P}_0)$ metastable level. This uncertainty was estimated by comparing our theoretical plasma rate coefficient of DR from the metastable level, with our theoretical plasma rate coefficient consisting of calculated metastable level DR and ground-level DR. For deriving an upper limit of this uncertainty, 12% and 88% of the ions were assumed to be in the metastable level and the ground level, respectively. We found an additional uncertainty ranging from 100% at a plasma temperature of $k_{\rm B}T = 0.01$ eV, 24% at 0.1 eV, 12% at 1.3 eV, 10% at 2.3 eV, 2% at 25 eV, 0.6% at 107 eV to 0.4% at $k_{\rm B}T = 1000$ eV. This means, that the uncertainty due to the fraction of metastable DR resonances in the measured spectrum is only critical at plasma temperatures which are far below the photoionized zone. In the photoionized zone this uncertainty is not so large and negligible in the collisionally ionized zone.

The total experimentally derived DR plasma rate coefficients for Fe VIII and for Fe IX are shown as thick solid lines in Figs. 7 and 8, respectively. They comprise the fitted low energy resonance strength, the remaining experimentally measured DR rate coefficients, and the unmeasured, theoretically calculated, but scaled to the experiment, contribution up to $n_{\rm max} = 1000$. The temperature dependent uncertainties due to field ionization, rate enhancement, and metastable levels added in quadrature to the experimental error yield the total uncertainty for the experimentally derived DR plasma rate coefficient, given at a 90%

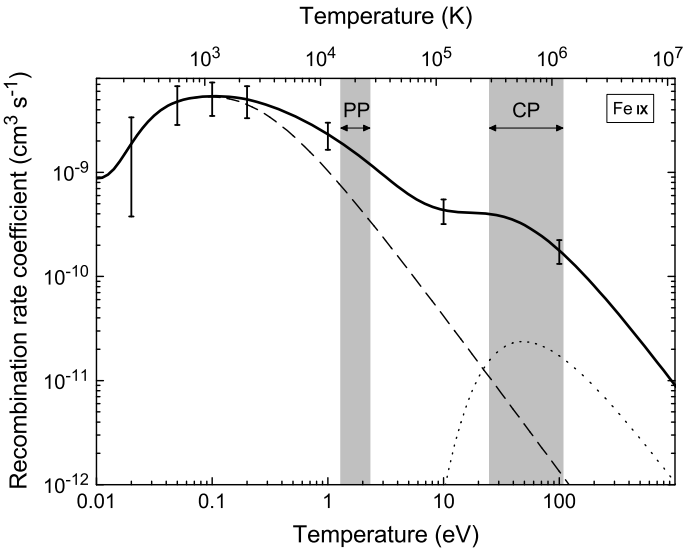

Fig. 8. Experimentally-derived Fe IX DR rate coefficient in a plasma (full curve) comprising DR associated with $3p^6 \rightarrow 3p^5\,3d$ core excitation (Fig. 4). The error bars denote the uncertainty of the absolute rate coefficient at a 90% confidence level. Temperature ranges are highlighted where Fe IX is expected to peak in abundance in photoionized and collisionally ionized plasmas. The estimated (unmeasured) DR contribution of levels with $n \geq 34$ (gray shaded area in Fig. 5) is shown by the dotted curve. The dashed curve shows the contribution of the 28 fitted low-energy resonances (lower panel of Fig. 6).

confidence level. For Fe VIII the total uncertainty is ≈54% at $k_B T = 0.01$ eV, ≈31% at 0.02 eV, and ≈25% at 0.05 eV and above. For Fe IX the total uncertainty is ≈106% at 0.01 eV, ≈80% at 0.02 eV, ≈40% at 0.05 eV, ≈35% at 0.1 eV, ≈34% at 0.2 eV, ≈29% at 1 eV, ≈27% at 10 eV, and less than 26% at 18 eV and above.

The AUTOSTRUCTURE DR plasma rate coefficients were derived by convolving the calculated cross sections with a Maxwell-Boltzmann electron energy distribution. These cross sections are not scaled to the experiment in contrast to the ones which were used for extrapolation of the experimental data.

5.2. Derivation of the RR plasma rate coefficients

RR plasma rate coefficients for Fe VIII and Fe IX for a Maxwellian electron energy distribution were derived from AUTOSTRUCTURE RR cross sections including excited levels up to $n_{max} = 1000$. They are shown as thick dotted lines in Figs. 9 and 10. As can be seen there, the DR plasma rate coefficient dominates over the RR plasma rate coefficient in a wide energy range for both ions. In the photoionized zone and the collisionally ionized zone, the RR plasma rate coefficient is one to two orders of magnitude smaller than the DR plasma rate coefficient.

5.3. Parameterization of plasma rate coefficients

For convenient use in astrophysical modeling codes the Fe VIII and Fe IX DR plasma rate coefficients α_P^{DR} were fitted using

$$\alpha_P^{DR}(T) = (T)^{-3/2} \sum_i c_i \exp(-E_i/T), \quad (4)$$

both for the experimental and the theoretical results. The resulting fitting parameters c_i and E_i are given in Table 3 for the experimentally derived Fe VIII and Fe IX and the theoretically calculated Fe VIII DR plasma rate coefficients. The fits deviate by less than 1% from the experimentally derived and the theoretically calculated DR plasma rate coefficients over 1 meV–100 keV (11.6 K–1.16×10^9 K). For a fit of the Fe IX AUTOSTRUCTURE DR plasma rate coefficient we refer the reader to the work of Badnell (2006a).

The theoretical Fe VIII and Fe IX RR plasma rate coefficients α_P^{RR} were fitted to the following functional form (Verner & Ferland 1996)

$$\alpha_P^{RR}(T) = A \left[\sqrt{\frac{T}{T_0}} \left(1 + \sqrt{\frac{T}{T_0}}\right)^{1-B'} \left(1 + \sqrt{\frac{T}{T_1}}\right)^{1+B'} \right]^{-1}, \quad (5)$$

where B' is (Gu 2003)

$$B' = B + C \exp\left(\frac{-T_2}{T}\right). \quad (6)$$

The fitting parameters A, B, T_0, T_1, C and T_2 are given in Table 4 for Fe VIII. The fitting coefficients for Fe IX were determined previously by Badnell (2006a). The fits deviate by less than 1% from the calculated results in the temperature range $(10 - 10^7)\,z^2$ K, where z is the ion charge before recombination.

6. Discussion

In Figs. 9 and 10 we compare the present experimental and AUTOSTRUCTURE calculated Fe VIII and Fe IX DR plasma rate coefficients. We also compare with the previously recommended DR plasma rate coefficients of Arnaud & Raymond (1992). We do not compare with any of the ad hoc changes proposed by Netzer (2004) and by Kraemer et al. (2004).

The agreement between the experimental and AUTOSTRUCTURE calculated DR plasma rate coefficients is mixed for Fe VIII. The experimentally-derived DR plasma rate coefficient is 5.4 times that of the theoretical one calculated with AUTOSTRUCTURE at $k_B T \approx 0.01$ eV, 3.2 at 0.1 eV, 1.7 at 1.1 eV, 1.3 at 2.1 eV, and they are equal at ≈3.3 eV. Above $k_B T = 3.3$ eV the experimentally-derived DR plasma rate coefficient is smaller than the AUTOSTRUCTURE one going down to a factor of 0.82 of the AUTOSTRUCTURE DR plasma rate coefficient at $k_B T \approx 8$ eV. It is between 0.82 and 0.85 above 8 eV. Looking at the AUTOSTRUCTURE calculations of TR associated with capture into $n = 3$ and of DR + TR associated with capture into $n \geq 4$ separately, we can see, that a calculation restricted to $n \geq 4$ DR would underestimate the experimental DR result strongly at temperatures where Fe VIII forms in a photoionized plasma. The experimentally derived DR plasma rate coefficient is 5.3 times that of the AUTOSTRUCTURE $n \geq 4$ DR + TR plasma rate coefficient at $k_B T = 1.1$ eV and 2.8 at 2.1 eV. This underestimate is because the AUTOSTRUCTURE calculation comprising of TR associated with capture into $n = 3$ dominates over the AUTOSTRUCTURE calculation comprising of DR + TR associated with capture into $n \geq 4$ in the temperature range $k_B T \approx 0.08$–2.7 eV. It is interesting to note that TR makes the dominant contribution to the plasma rate coefficient in the photoionized zone.

For Fe IX the agreement between the experimental and the AUTOSTRUCTURE calculated DR plasma rate coefficient is not as good as for Fe VIII. The experimentally-derived Fe IX DR plasma rate coefficient exceeds the theoretical one over the whole temperature range, despite the fact, that near the $3p^5\,3d\,{}^1P_1^\circ$ series limit at $\hat{E} = 72.5$ eV the theoretical DR

Table 3. Parameters c_i $\left(\mathrm{cm^3\,s^{-1}\,K^{3/2}}\right)$ and E_i (K) for the fits of Eq. (4) to the experimentally derived Fe VIII and Fe IX and theoretically calculated Fe VIII DR plasma rate coefficients.

	Experiment				Theory	
	Fe VIII		Fe IX		Fe VIII	
i	c_i	E_i	c_i	E_i	c_i	E_i
1	5.978[−7]	8.385[0]	4.777[−7]	9.034[0]	3.113[−7]	9.499[1]
2	8.939[−7]	9.922[1]	1.231[−6]	1.128[2]	8.783[−7]	3.031[2]
3	1.640[−5]	5.234[2]	5.055[−5]	6.624[2]	3.956[−6]	7.878[2]
4	9.598[−5]	1.579[3]	3.413[−4]	1.143[3]	5.539[−5]	2.080[3]
5	1.105[−4]	4.489[3]	1.625[−3]	3.926[3]	9.422[−5]	7.209[3]
6	7.299[−4]	2.102[4]	3.873[−3]	1.300[4]	9.343[−4]	3.159[4]
7	3.858[−3]	9.778[4]	6.438[−3]	4.684[4]	5.296[−3]	1.020[5]
8	2.476[−2]	3.353[5]	6.970[−2]	2.670[5]	1.780[−2]	2.803[5]
9	1.789[−1]	8.081[5]	2.925[−1]	7.358[5]	2.269[−1]	7.840[5]

Numbers in square brackets denote powers of 10.

Table 4. Parameters for the fit applying Eqs. (5) and (6) to the theoretical Fe VIII RR plasma rate coefficient.

A $(\mathrm{cm^3\,s^{-1}})$	B	T_0 (K)	T_1 (K)	C	T_2 (K)
1.121[−9]	0.7407	3.753[1]	2.418[7]	0.0720	3.280[5]

Numbers in square brackets denote powers of 10.

merged-beams rate coefficient was larger than the experimentally derived one. The experimentally-derived DR plasma rate coefficient is 1152 times that of the theoretical one calculated with AUTOSTRUCTURE at $k_\mathrm{B}T$ = 0.01 eV, 3.34 at 0.1 eV, 1.7 at 1.3 eV, 1.5 at 2.3 eV, 1.51 at 25 eV, 1.25 at 107 eV, 1.19 at 1000 eV, and 1.18 above 1000 eV.

As seen in Figs. 9 and 10 the DR plasma rate coefficients of Arnaud & Raymond (1992) are orders of magnitude below the experimentally derived rate coefficients in the zones where Fe VIII and Fe IX form in a photoionization equilibrium. This is not surprising as the Fe VIII and Fe IX DR rate coefficients given in Arnaud & Raymond (1992) were originally calculated with the Burgess formula and scaled to the results of Hahn (1989), neither of which take into account the DR resonances important at low electron-ion collision energies. As one can see, for Fe VIII our experimentally-derived DR plasma rate coefficient is 19.7 times that of the Arnaud & Raymond (1992) recommended one at $k_\mathrm{B}T$ = 10 eV, 1.4 at 50 eV, 1.2 at 100 eV and between 1.06–1.08 in the energy range 10^3–10^5 eV. For Fe IX our experimentally-derived DR plasma rate coefficient is 70.8 times that of the Arnaud & Raymond (1992) recommended one at $k_\mathrm{B}T$ = 10 eV, 2.6 at 50 eV, 2.0 at 100 eV and between 1.51–1.55 in the energy range 10^3–10^5 eV.

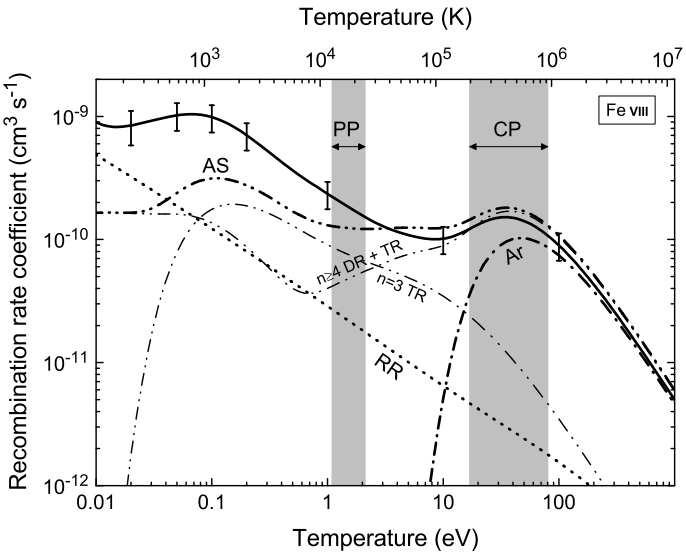

Fig. 9. Comparison of the experimentally-derived and theoretical Fe VIII recombination rate coefficients in a plasma. The thick full line shows the experimentally-derived DR plasma rate coefficient comprising $\Delta n^* = 0$ DR (Fig. 1), $\Delta n^* = 1$ and $\Delta n^* = 2$ DR (Fig. 2), and the theoretical estimate for the unmeasured contribution of levels with $n \geq 32$ (gray area in Fig. 3). The error bars denote the uncertainty in the absolute rate coefficient. The thick dash-dot-dotted line labeled AS shows the AUTOSTRUCTURE DR plasma rate coefficient comprising all DR contributions associated with capture into $n = 3$ and capture into $n \geq 4$ (thin dash-dot-dotted lines labeled "$n = 3$ TR" and "$n \geq 4$ DR + TR", respectively). Also shown is the recommended DR rate coefficient of Arnaud & Raymond (1992, thick dash-dotted line labeled Ar). The thick dotted curve labeled RR shows the AUTOSTRUCTURE calculated RR plasma rate coefficient. Temperature ranges are highlighted and labeled PP and CP, respectively, where Fe VIII is expected to peak in abundance in photoionized and collisionally ionized plasmas.

7. Conclusions

The presented experimental and theoretical results for the DR, TR, and RR rate coefficients of potassium-like Fe VIII ions forming calcium-like Fe VII and of argon-like Fe IX forming potassium-like Fe VIII have shown that the suggestions by Netzer (2004) and Kraemer et al. (2004) to increase the iron M-shell DR rate coefficients at electron temperatures where these ions form in photoionized plasmas were pointing in the right direction. Our experimentally-derived DR + TR rate coefficients are orders of magnitude larger than the recommended DR values from the compilation of Arnaud & Raymond (1992). A similar discrepancy has already been found for aluminium-like Fe XIV (Schmidt et al. 2006) and magnesium-like Fe XV (Lukić et al. 2007) and can be expected for the remaining iron M-shell ions. This is because the earlier theoretical calculations were performed for high-temperature plasmas and did not include the DR channels important for low-temperatures plasmas. Since our DR + TR results are also about an order of magnitude larger than the RR rate coefficients this has important consequences for the modeling and interpretation of X-ray spectra from AGN and other cosmic sources.

Our results show that DR rate coefficients for medium charged iron M-shell ions in photoionized plasmas are strongly

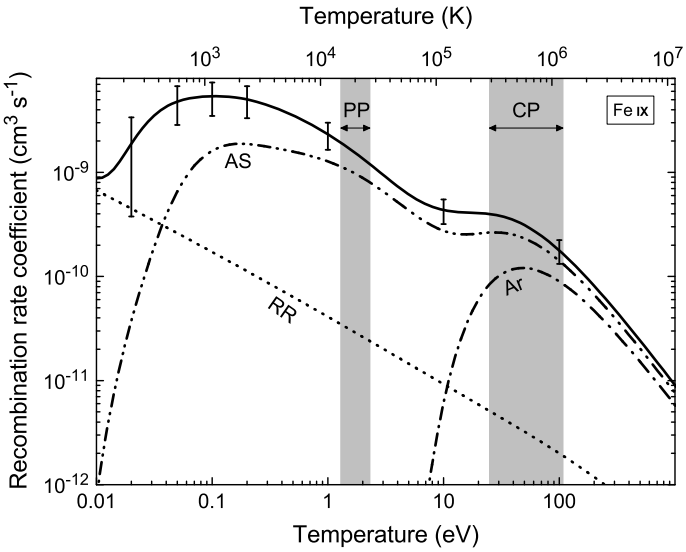

Fig. 10. Comparison of the experimentally-derived and theoretical Fe IX recombination rate coefficients in a plasma. The thick full line shows the experimentally-derived DR rate coefficient comprising $\Delta n^* = 0$ DR (Fig. 4) and the theoretical estimate for the unmeasured contribution of levels with $n \geq 34$ (gray area in Fig. 5). The error bars denote the uncertainty in the absolute rate coefficient. The recent AUTOSTRUCTURE DR and RR calculations by Badnell (2006a) are represented by thick dash-dot-dotted line labeled AS and thick dotted line labeled RR, respectively. Also shown is the recommended DR rate coefficient of Arnaud & Raymond (1992, thick dash-dotted line labeled Ar). Temperature ranges are highlighted and labeled PP and CP, respectively, where Fe IX is expected to peak in abundance in photoionized and collisionally ionized plasmas.

influenced by resonances at low electron ion collision energies. This is in line with previous findings for more highly charged iron M-shell ions (Müller 1999; Lukić et al. 2007; Schmidt et al. 2006). The theoretical challenge is the accurate prediction of these low-energy resonances which are subject to strong correlation effects. The difficulty to describe these resonances sufficiently well is reflected by the significant deviation of the theoretical plasma rate coefficients from the experimental results at low temperatures. Therefore, for the time being storage-ring experiments remain a vitally needed source for recombination rate coefficients in photoionized plasmas. We are in the process of carrying out DR measurements for additional Fe M-shell ions. As these data become available we recommend that these experimentally derived DR rate coefficients be incorporated into AGN spectral models in order to produce more meaningful interpretations of the astrophysical data.

Acknowledgements. We gratefully acknowledge the excellent support by the MPI-K accelerator and storage-ring crews. This work was supported by the German federal research-funding agency DFG under contract no. Schi 378/5. M. L., D. V. L., and D. W. S. were supported in part by the NASA Astronomy and Physics Research and Analysis program, and the NASA Solar and Heliosperic Physics program.

References

Arnaud, M., & Raymond, J. 1992, ApJ, 398, 394
Badnell, N. R. 1986, J. Phys. B, 19, 3827, http://amdpp.phys.strath.ac.uk/autos/
Badnell, N. R. 2006a, ApJ, 651, L73
Badnell, N. R. 2006b, J. Phys. B, 39, 4825
Badnell, N. R. 2006c, ApJS, 167, 334
Badnell, N. R., O'Mullane, M. G., Summers, H. P., et al. 2003, A&A, 406, 1151
Behar, E., Sako, M., & Kahn, S. M. 2001, ApJ, 563, 497
Behar, E., Rasmussen, A. P., Blustin, A. J., et al. 2003, ApJ, 598, 232
Bryans, P., Badnell, N. R., Gorczyca, T. W., et al. 2006, ApJS, 167, 343
Burgess, A. 1965, ApJ, 141, 1588
Fogle, M., Eklöw, N., Lindroth, E., et al. 2003, J. Phys. B, 36, 2563
Gallo, L. C., Boller, T., Brandt, W. N., Fabian, A. C., & Vaughan, S. 2004, A&A, 417, 29
Grieser, M., Blum, M., Habs, D., et al. 1991, Advanced Stacking Methods Using Electron Cooling at the TSR Heidelberg, in Proc. 19th Inter. Sympos. on Cooler Rings and Their Applications, Tokyo, Japan, November 5–8, 1990, ed. T. Katayama, & A. Noda (Singapore: World Scientific), 190
Gu, M. F. 2003, ApJ, 589, 1085
Gwinner, G., Hoffknecht, A., Bartsch, T., et al. 2000, Phys. Rev. Lett., 84, 4822
Hahn, Y. 1989, J. Quant. Spectrosc. Radiat. Transfer, 41, 315
Hörndl, M., Yoshida, S., Wolf, A., et al. 2006, Phys. Rev. A, 74, 052712
Jacobs, V. L., Davis, J., Kepple, P. C., & Blaha, M. 1977, ApJ, 211, 650
Kallman, T. R., Palmeri, P., Bautista, M. A., Mendoza, C., & Krolik, J. H. 2004, ApJS, 155, 675
Kaspi, S., Brandt, W. N., George, I. M., et al. 2002, ApJ, 574, 643
Kaspi, S., Netzer, H., Chelouche, D., et al. 2004, ApJ, 611, 68
Kilgus, G., Habs, D., Schwalm, D., et al. 1992, Phys. Rev. A, 46, 5730
Kraemer, S. B., Ferland, G. J., & Gabel, J. R. 2004, ApJ, 604, 556
Krongold, Y., Nicastro, F., Elvis, M., et al. 2005, ApJ, 620, 165
Lampert, A., Wolf, A., Habs, D., et al. 1996, Phys. Rev. A, 53, 1413
Lestinsky, M., Lindroth, E., Orlov, D. A., et al. 2008, Phys. Rev. Lett., 100, 033001
Linkemann, J., Kenntner, J., Müller, A., et al. 1995, Nucl. Instrum. Methods B, 98, 154
Lukić, D., Savin, D. W., Schnell, M., et al. 2007, ApJ, 664, 1244
Müller, A. 1999, Int. J. Mass Spectrom., 192, 9
Müller, A., & Wolf, A. 1997, Heavy ion storage rings, in Accelerator-based atomic physics techniques and applications, ed. J. C. Austin, & S. M. Shafroth (Woodbury: AIP Press), 147
Netzer, H. 2004, ApJ, 604, 551
Netzer, H., Kaspi, S., Behar, E., et al. 2003, ApJ, 599, 933
Nikolić, D., Gorczyca, T. W., Fu, J., Savin, D. W., & Badnell, N. 2007, Nucl. Instrum. Methods B, 261, 145
Orban, I., Glans, P., Altun, Z., et al. 2006, A&A, 459, 291
Pastuszka, S., Schramm, U., Grieser, M., et al. 1996, Nucl. Instrum. Methods A, 369, 11
Pindzola, M. S., Badnell, N. R., & Griffin, D. C. 1992, Phys. Rev. A, 46, 5725
Poth, H., Seligmann, B., Schwab, W., et al. 1988, Hyperfine Interact., 44, 259
Pounds, K., Reeves, J., O'Brien, P., et al. 2001, ApJ, 559, 181
Pounds, K. A., Reeves, J. N., King, A. R., & Page, K. L. 2004, MNRAS, 350, 10
Ralchenko, Y., Jou, F.-C., Kelleher, D. E., et al. 2007, NIST Atomic Spectra Database (version 3.1.1) (Gaithersburg, MD: National Institute of Standards and Technology), http://physics.nist.gov/asd3
Sako, M., Kahn, S. M., Behar, E., et al. 2001, A&A, 365, L168
Savin, D. W., Gwinner, G., Grieser, M., et al. 2006, ApJ, 642, 1275
Schippers, S. 2008, J. Phys. Conf. Ser., in press [arXiv:0808.3366]
Schippers, S., Bartsch, T., Brandau, C., et al. 1998, J. Phys. B, 31, 4873
Schippers, S., Müller, A., Gwinner, G., et al. 2001, ApJ, 555, 1027
Schippers, S., Kieslich, S., Müller, A., et al. 2002, Phys. Rev. A, 65, 042723
Schippers, S., Schnell, M., Brandau, C., et al. 2004, A&A, 421, 1185
Schmidt, E. W., Schippers, S., Müller, A., et al. 2006, ApJ, 641, L157
Schmidt, E. W., Bernhardt, D., Müller, A., et al. 2007, Phys. Rev. A, 76, 032717
Schnell, M., Gwinner, G., Badnell, N. R., et al. 2003, Phys. Rev. Lett., 91, 043001
Seaton, M. J., & Storey, P. J. 1976, Di-Electronic Recombination, in Atomic Processes and Applications, ed. P. G. Burke, & B. L. Moiseiwitsch (Amsterdam: North-Holland Publishing Company), 133
Sprenger, F., Lestinsky, M., Orlov, D. A., Schwalm, D., & Wolf, A. 2004, Nucl. Instrum. Methods A, 532, 298
Steenbrugge, K. C., Kaastra, J. S., de Vries, C. P., & Edelson, R. 2003, A&A, 402, 477
Verner, D. A., & Ferland, G. J. 1996, ApJS, 103, 467
Wolf, A., & Gwinner, G. 2003, Hyperfine Interact., 146/147, 5
Wolf, A., Buhr, H., Grieser, M., et al. 2006, Hyperfine Interact., 172, 111
Woods, D. T., Shull, J. M., & Sarazin, C. L. 1981, ApJ, 249, 399